UNIQUE CHARACTERIZATION OF SPATIOTEMPORAL NEURONAL NETWORK ACTIVITY

A PREPRINT

Sarita S. Deshpande*
Committee on Neurobiology
Section of Pediatric Neurology
Interdisciplinary Scientist Training Program
University of Chicago
Chicago, IL 60637

Graham Smith*
Committee on Computational Neuroscience
Section of Pediatric Neurology
University of Chicago
Chicago, IL 60637

Wim van Drongelen
Committee on Computatonal Neuroscience
Committee on Neurobiology
Section of Pediatric Neurology
University of Chicago
Chicago, IL 60637
wvandron@peds.bsd.uchicago.edu

August 17, 2021

ABSTRACT

We apply the Triple Correlation Uniqueness (TCU) theorem to the most basic representation of network spiking activity, the raster, to prove that third-order (triple) correlation uniquely characterizes spiking activity in the brain. As a consequence, the three-node (triple) motifs comprising the triple correlation are fundamental building blocks of neuronal activity. By analysing the putative flow of information in these motifs, we group all possible motifs into fourteen motif-classes. These motif-classes embody well-known and well-studied properties in neuroscience, e.g. spike rate, local dynamics, synchrony, feedback, feedforward, convergence, and divergence. We show that motifs with some of these properties—divergence, convergence, and feedforward—are far more prevalent in the triple correlation; and thus, these properties contribute more to characterizing neural activity than do the other properties. In the frequency domain, the triple correlation is the bispectrum, which characterizes the phase-relationship between spike trains and the relationships between frequency bands. We apply these analyses to example rasters to illustrate the dependence of our characterization on the firing patterns underlying neural activity.

Keywords Third-Order Autocorrelation · Bispectrum · Julesz Conjecture · Triple Correlation Uniqueness Theorem · Network Motifs · Raster Plot

1 Introduction

Researchers use increasingly diverse modalities to record neuronal activity, and many more methods to analyse the resulting patterns. Across all these various modalities and analytical methods, though, the raw representation of the spiking activity has been the same for decades: the raster plot. Many of the analytical approaches boil down to clever applications of quantitative relationships, e.g. correlations, between or within the spike trains in a population, i.e. the rows of the raster. For one particularly useful example, one takes the cross-correlations between spike trains and from

*Authors contributed equally.

those derives edges in a graph representation of the underlying neuronal network, thus constructing a functional connectivity network. However, we can take a more direct approach by treating the raster as an image. Specifically, we apply the Triple Correlation Uniqueness (TCU) theorem to rasters, directly deriving a theoretically complete correlation analysis and implicitly the underlying fundamental building blocks of brain activity.

The TCU theorem has a long history in optical science, introduced by Bartelt et al. (1984), then refined and named by Yellot and Iverson (1992). Yellott (1993) used it to state a corrected version of the then-disproven Julesz conjecture (Julesz, 1962; Julesz et al., 1973). Julesz had conjectured that the brain cannot spontaneously discriminate between images with identical second-order statistics. With the TCU theorem, Yellott proved that any human observer is unable to distinguish between images with identical third-order statistics, for the simple reason that such images are identical (up to translation).

Here, we bring the TCU theorem into the heart of neuroscience to characterize image-like spike rasters and thus to characterize neuronal network activity patterns. We begin by describing the triple correlation (c_T) and its frequency domain equivalent, the bispectrum (C_T). Next, we give a summary of the proof of the uniqueness of c_T for its associated image. Then, we examine the triple correlation function in terms of its constituent parts, discuss the consequences of the uniqueness result for motifs, and categorize these motifs according to their relevance to neural information processing. Finally, we simulate multi-unit spike activity recordings to demonstrate how the application of these analyses characterize the underlying firing pattern of neuronal activity.

2 Triple Correlation and the Bispectrum

Our key insight is that since the spike raster is an image, its triple correlation is unique. Due to this uniqueness, we need not seek beyond third-order for higher-order relationships amongst spike trains. Put another way, the relationships among triplets of spikes constitute the fundamental building blocks of a complete statistical account of spiking activity. This statistical account is "complete" in the sense that the spiking activity can be recovered in its entirety from the complete triple correlation function (see "Reconstruction Algorithms for Finite Images" in Yellott & Iverson, 1992).

2.1 Defining the raster and triple correlation

We represent neuronal activity as a typical two-dimensional raster, $r(\boldsymbol{\sigma}) = r(n, t)$, where n is neuron location, t is time, and $\boldsymbol{\sigma} = (n, t)$ is a vector of both for notational simplicity below. We will refer to neuron number rather than location to emphasize that we have not imposed any particular order, with caveats discussed later. Throughout, we will assume that the raster is binary (black and white, cf. Fig. 1), so that $r(n, t) = 1$ if neuron n fires at time t, and $r(n, t) = 0$ otherwise. We note that everything below works just as well for any finite number of colors (Yellot, 1993), such as would be the case with discretized local field potential (LFP) or EEG recordings. Even a colorful raster is still an image.

Triple correlation, c_T, or third-order autocorrelation, is the next highest order extension of the usual pairwise correlation. The pairwise correlation is a function of the lag $\boldsymbol{\lambda} = (\nu, \tau)$ between two pixels at locations $\boldsymbol{\sigma}_0$ and $\boldsymbol{\sigma}_1$; the triple correlation is a function of the lags between three pixels at locations $\boldsymbol{\sigma}_0, \boldsymbol{\sigma}_1$, and $\boldsymbol{\sigma}_2$. Concretely c_T is a function of $\boldsymbol{\lambda}_1$ and $\boldsymbol{\lambda}_2$, the spatiotemporal lags from a base pixel $r(\boldsymbol{\sigma}_0)$ (implicitly at lag $\lambda_0 = 0$) to two other pixels, $r(\boldsymbol{\sigma}_1)$ and $r(\boldsymbol{\sigma}_2)$ at lags $\boldsymbol{\lambda}_1 = \boldsymbol{\sigma}_1 - \boldsymbol{\sigma}_0$ and $\boldsymbol{\lambda}_2 = \boldsymbol{\sigma}_2 - \boldsymbol{\sigma}_0$. To compute this function for a given lag-triplet $\boldsymbol{\lambda}_1, \boldsymbol{\lambda}_2$, we find the number of pixel-triplets where all the pixels in the triplet are firing, i.e. $r(\boldsymbol{\sigma}_0)r(\boldsymbol{\sigma}_1)r(\boldsymbol{\sigma}_2) = 1$, and the distances between the pixels fit the lag-triplet, i.e. $\boldsymbol{\lambda}_1 = \boldsymbol{\sigma}_1 - \boldsymbol{\sigma}_0$ and $\boldsymbol{\lambda}_2 = \boldsymbol{\sigma}_2 - \boldsymbol{\sigma}_0$. When scaled by the number of possible base pixels, this quantity is the triple correlation evaluated at the given spatiotemporal lags.

2.2 Triple correlation uniqueness theorem

Our key insight follows from the TCU theorem (see Bartelt, 1984; Yellot and Iverson, 1992). In the Supporting Materials (Section A), we include a full proof for the spatiotemporal version, which is a natural extension of Yellott and Iverson's proof. Here, we provide an overview.

The TCU theorem holds because we can treat the spike raster (or any finite image) as a probability density function. We assume that any spike raster takes only values that are finite. We can normalize all the pixels' luminances (i.e. the spikes) such that the sum across the whole raster is one. And, finally, all the raster's pixels are non-negative. Together, these facts satisfy the definition of a probability density function.

We consider the Fourier transform of the triple correlation, $\mathscr{F}[c_T] = C_T$, the raster's bispectrum. We aim to show that given two identical bispectra, the rasters that produced those bispectra are the same, up to translation of the raster. Since we can treat the raster as a probability density function, its Fourier transform R is a characteristic function.

Characteristic functions have several convenient properties, including that they are Hermitian and nonzero near the origin. Thanks to the latter property, when we set two bispectra of potentially different rasters R and S equal to each other, we can divide through to find that the ratio R/S is equal to the complex exponental function, which means $R(\hat{\boldsymbol{\lambda}}) = S(\hat{\boldsymbol{\lambda}})\exp(j\mathbf{k}\cdot\hat{\boldsymbol{\lambda}})$ where $\mathbf{k}$ is a constant vector of the same length as $\hat{\boldsymbol{\lambda}}$. In the spatiotemporal domain, this means $r(\boldsymbol{\lambda}) = s(\boldsymbol{\lambda}+\mathbf{k})$. In other words, the rasters are the same except one may be translated versus the other.

2.3 Computing the triple correlation

For computational applications, we consider third-order correlation analysis applied to a discrete raster with neuron rows n, `1:N`, and time columns t, `1:T`, where each pixel $r(n,t)$ is filled with a 0 (white for no activity) or 1 (black for spike). The complete triple correlation function, while formally requisite, incurs substantial computational cost while adding increasingly noisy information. We limit our computation to lag windows $-W_t : W_t$ and $-W_n : W_n$ chosen such that two local synaptic connections could not take longer than W_t, and two neurons are unlikely to be connected further than W_n. Given this restricted lag window, we do not zero pad our raster (as in Yellott & Iverson, 1992) but instead restrict our calculation to a subset of the raster within bands given by W_t and W_n. In this case, discrete equivalent cd_T of the triple correlation expression c_T (Equation A1) is

$$cd_T(n_1,t_1,n_2,t_2) = \frac{1}{\#(W_n,W_t,N,T)} \sum_{t=1+W_t}^{T-W_t} \sum_{n=1+W_n}^{T-W_n} r(n,t)r(n+n_1,t+t_1)r(n+n_2,t+t_2). \tag{1}$$

Note that the lags should be symmetric about zero, because unlike the pairwise correlation, the triple correlation is even symmetric in four variables, not one, so we only have the symmetry $cd_T(n_1,t_1,n_2,t_2) = cd_T(-n_1,-t_1,-n_2,-t_2)$. Further, to avoid spurious combinatorial assignations of importance to either time or space, we have chosen to set $W_t = W_n$.

We scale by the number of triplets in the summation

$$\#(W_n,W_t,N,T) = (T-2W_t)(N-2W_n). \tag{2}$$

Equations (1) and (2) were used in our simulations presented in Figs. 2 and 3. In these simulations, we used raster dimensions of 150×150 (neuron # $\times$ time step) with $W_n = 7$ and $W_t = 7$.

3 Triple Correlation and Network Motifs

The triplet building blocks of the triple correlation function provide a theoretical foundation for the study of triplet motifs now prevalent in neuroscience. Here, we aim to explore this intuition and to more broadly extract meaning from these theoretically deduced objects. We might wonder about the complexity of this much higher dimensional object that uniquely represents the raster. So we will additionally count the number of objects represented at each step of the computation, both to act as a sanity check the reader's intuition and to illustrate our descent from the combinatorial explosion caused by considering all spatiotemporal triplets down to the much fewer and more meaningful information flow motif-classes that we derive.

3.1 Lag motifs comprise triple correlation

As seen in the previous section, the starting point for the triple correlation calculation is the spatiotemporal triplet $(\boldsymbol{\sigma}_0,\boldsymbol{\sigma}_1,\boldsymbol{\sigma}_2)$. In the event that there are spikes at all three locations in this triplet, i.e. $r(\boldsymbol{\sigma}_0)r(\boldsymbol{\sigma}_1)r(\boldsymbol{\sigma}_2) = 1$, then it is a spike triplet and contributes through summation to the relevant triple correlation value, $c_T(\boldsymbol{\sigma}_1-\boldsymbol{\sigma}_0,\boldsymbol{\sigma}_2-\boldsymbol{\sigma}_0) = c_T(\boldsymbol{\lambda}_1,\boldsymbol{\lambda}_2) = \#(\boldsymbol{\lambda}_1,\boldsymbol{\lambda}_2)^{-1}\sum_{\boldsymbol{\sigma}_0} r(\boldsymbol{\sigma}_0)r(\boldsymbol{\sigma}_0+\boldsymbol{\lambda}_1)r(\boldsymbol{\sigma}_0+\boldsymbol{\lambda}_2)$. Since the spike triplet is one example of many that contribute to the triple correlation with those given lags, we say the spike triplet is part of the lag triplet motif given by $(0,\boldsymbol{\lambda}_1,\boldsymbol{\lambda}_2)$, or simply the lag motif given by $(\boldsymbol{\lambda}_1,\boldsymbol{\lambda}_2)$ since 0 and triple are always implied. Note that these triplets and motifs are undirected.

The total number of spatiotemporal triplets (i.e. potential spike triplets) is the sum of the scaling factor $\#(\boldsymbol{\lambda}_1,\boldsymbol{\lambda}_2)$ over all lags within the bounds of the raster. In the zero padded case, the number of such triplets is a straightforward $\binom{NT}{3}$. Since we do not zero pad (and further restrict our lag window to a causally plausible extent), we use (2) to calculate that the number of such triplets is $\sum_{\boldsymbol{\lambda}_1,\boldsymbol{\lambda}_2}\#(\boldsymbol{\lambda}_1,\boldsymbol{\lambda}_2) = 1,139,062,500$ in our 150×150 raster using a lag windows of `-7:7`. Of these many triplets, each falls into one of `length(-7:7)^4`$= 50,625$ lag motifs (i.e. all calculated entries of the triple correlation).

3.2 Classifying lag motifs by information flow

These lag motifs constitute the raw components of the triple correlation, entirely due to the mathematics, with no respect to what these components mean. However, as neuroscientists, we find most interesting the potential *causation* suggested by the relationships amongst the raster's spikes. We aim to incorporate causation, then, to reduce the $50,625$ lag motifs in the raw triple correlation to something both more managable and meaningful. The simplest classification is into negative lags (anti-causal), zero lags (acausal), and positive lags (putatively causal). While we understand that correlation does not imply causation, we follow this line of reasoning as frequently done in mutual information, correlation, and Granger causality studies in neuroscience network analysis. In choosing to classify the zero lags together, we implicitly assume that the time bin of our raster is sufficiently large as to encompass any delay due to synaptic transmission, thus making the zero lag the only lag encompassing a definitively acausal period. In space, zero is also meaningful, as it indicates a spike from the same neuron. On the other hand, negative versus positive spatial lag may or may not be meaningful, depending on whether the neurons are ordered in a meaningful way. For completeness, we distinguish negative, zero, and positive lags in both time and space. We enumerate the resulting classification in Table D2, and prove that our enumeration is exhaustive in the Supporting Materials (Section D). We find that this classification results in 169 lag motifs.

We adopt the preceding interpretation to reduce these 169 lag motifs into 14 information flow patterns through the following observations: 1) the order of our labeling of the lag motif as $(0, \lambda_1, \lambda_2)$ is meaningless—we could just as well permute to $(\lambda_1, 0, \lambda_2)$, so, for example lag motifs 2.1, 2.2, 3.1, and 3.2 of Table D2 are all equivalent; 2) in our arbitrary spatial ordering, only zero versus non-zero spatial lag has meaning; and 3) negative, zero, and positive temporal lag all have distinct meanings, so e.g. IX and X are distinct in Fig. 1.

In Fig. 2, we depict the potential contributions to the triple correlation function of each of the information flow patterns. This potential contribution is measured as the number of spike triplets classified under each information flow pattern's motif-class in a raster with all possible spikes (completely black). In general, the more distinct neurons and time bins involved in a pattern, the more potential triplets falling under that pattern's motif-class. This is roughly reflected by the number of blue arrows in the motif-class' representation in Fig. 1.

3.3 Properties of information flow

The information flow patterns finally give meaning to the building blocks of the triple correlation, i.e. the building blocks of neural activity. Interpretations in terms properties that are well-studied in neuroscience are given in Table 1. With such properties, we interface with extant literature on network motifs: a typical aim of network motif research is to find increased prevalence of motifs with apparent functional properties such as feedback (Milo et al., 2002). The key difference between our approach to deriving information flow patterns compared with those that are derived from known functional and structural network motifs is that current research usually constructs network connections via pairwise relationships such as cross-correlations, and then finds motifs in the resulting graph. Instead, we infer information flow directly from the triple correlation. Note that our motifs correspond to unidirectional up-to-three-neuron network motifs.

4 Application to Neuronal Firing Patterns

We simulated neuronal action potential activity in a network and presented the action potential or spike as a black dot in a spatiotemporal plot, the spike raster (note that the raster representations in figures include white space between spikes for legibility, but the rasters analysed did not include such spacing). For a given raster size (150 time-steps and 150 neuron-locations), we can determine the maximum potential contribution (Fig. 2B) for each of the 14 information flow patterns as shown in Fig. 1 and Table 1 by calculating the unscaled triple correlation (Equation (1)) of a raster with a spike at every position.

Using the same raster size, we simulated a more interesting pattern, where not all positions are occupied by a spike (e.g. Fig 2A). From this raster, we calculated the unscaled triple correlation to determine the actual contribution for each of the flow patterns (Fig. 2C) and the ratio between the actual and potential contribution (Fig 2D). We intuitively expect these ratios to reflect structure in the putative information flow of the underlying network. To explore this intuition, we calculated the same ratios for various different patterns: frequency $f = 0.12$ AU in Fig.3A, a phase shift in Fig. 3B, and additional tonic firing in Fig. 3C. We also simulated the effect of noise by varying the signal-to-noise ratios (SNR) in Fig. 3D-F. In each case, we also compared the ratios to those of pure noise.

Comparing the pure noise ratios to the ratios from structured rasters reveals a difference: the synchronous oscillating neurons had enhanced contributions from motif-classes involving synchrony (IV, V, VII, VIII, XII, XIII). Introducing phase shifting slightly increased spike propagation (VI) and the related (IX, X, XI), and decreased synchrony. Adding

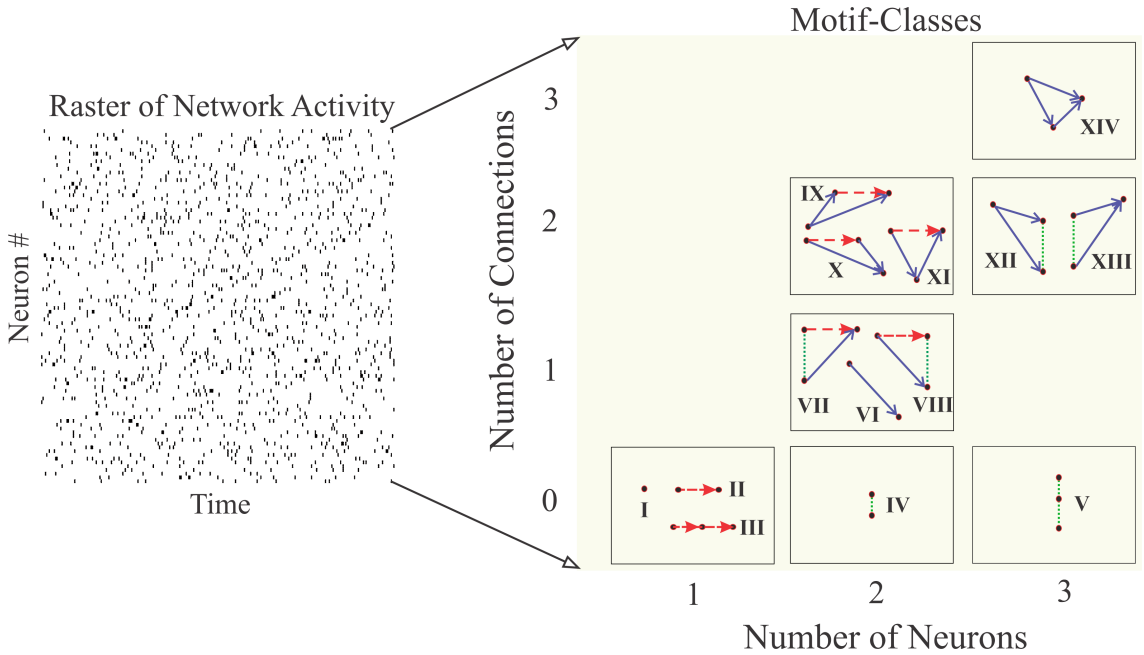

Figure 1: **Application of the 14 motif-classes to the spike raster**. The motif-classes summarized in Table 1 can be applied to a raster plot (left panel). In this case, we place three nodes in the raster's spatiotemporal plane (time on the horizontal axis and neuron# or location on the vertical axis) representative for the raster (right panel) and indicate time delays by arrows. Absence of a time-lag between different nodes indicates synchronous firing by multiple neurons and is represented by a vertical stippled line without an arrow head (e.g. IV). Absence of spatial-lag with a non-zero time-lag indicates repeated spiking within a single neuron and is represented by a dashed line with an arrow head (e.g. II). Non-zero lags in both time and space are indicated by solid arrows (e.g. VI).

Table 1: **Neuronal processing properties from Fig. 1 and their potential contributions to the triple correlation. Property**: Neuronal processing properties are listed in the first column. **Motif-Classes**: Motif-classes from Fig. 1 that incorporate the property are listed in the second column. **Characteristic Classes** the information flow motif-classes that purely incorporate the property [* or may purely incorporate one of multiple properties]. Note that some properties imply others, e.g. feedback includes spike propagation, so XI includes both feedback and spike propagation, but we still say it is the pure feedback motif. **Potential Contribution**: The proportion the triple correlation that may be purely determined by this property. We calculate this by finding in an always-firing raster (completely black) the proportion of lag motifs in the characteristic class(es) of the property. Note that the potential contributions do not add up to 100% because there is overlap in the characteristic classes. Moreover, without the overlap, these properties' potential contribution would sum to less than 100%. There are motif-classes that are not characteristic classes, so there are motif-classes that are not entirely described by any one property.

Property	**Motif-Classes**	**Characteristic Classes**	**Potential contribution**
Spike Rate	(all)	I	$< 0.01\%$
Local Dynamics	II, III, VII, VIII, IX, X, XI	II, III	0.4%
Synchrony	IV, V, VII, VIII, XII, XIII	IV, V	0.4%
Spike Propagation	VI, VII, VIII, IX, X, XI, XII, XIII, XIV	VI	1%
Feedback	XI	XI	5.0%
Feedforward	XIV	XIV*	65%
Divergence	XII, XIV	XII, XIV*	73%
Convergence	XIII, XIV	XIII, XIV*	73%

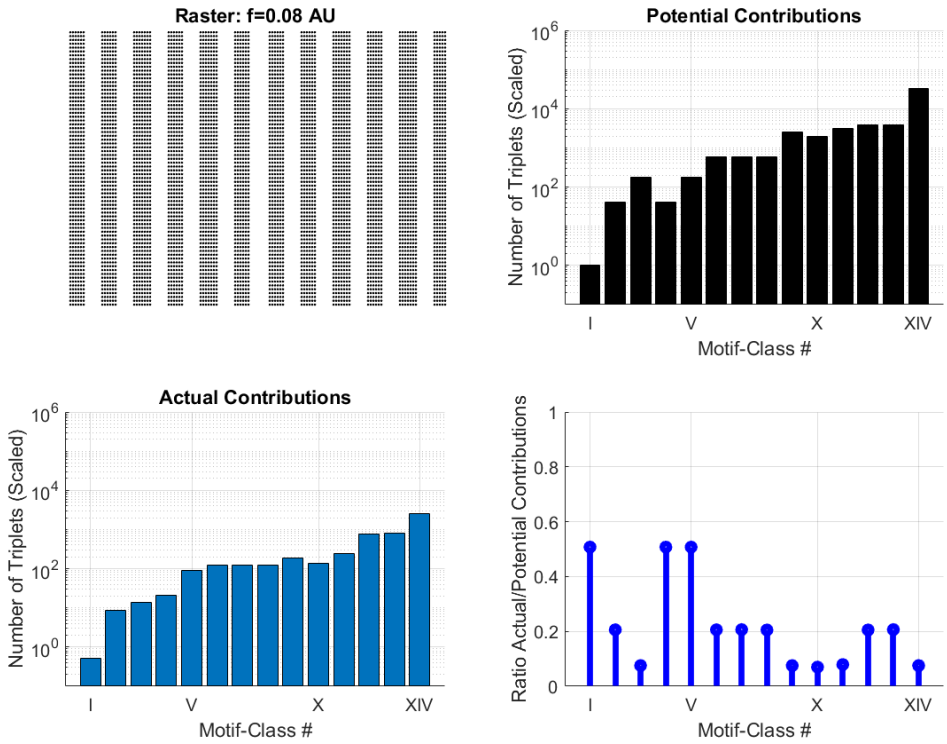

Figure 2: **Potential contribution of each motif-class to the raster's triple correlation.** A) The 150×150 spike raster plot has a frequency of 0.08 AU. B) The potential contribution (ordinate) for each of the 14 motif-classes in Fig. 1 (abscissa) to the triple correlation of a 150×150 raster plot using a lag window size of 15 for neuron# and 15 for time. In this case, the outcomes are the maximal possible contributions since they are based on a spike from every neuron at every time. C) The actual contributions of the 14 motif-classes for a periodic raster pattern shown in Panel A. D) The ratio between actual (Panel C) and potential contributions (Panel B) for the raster shown in Panel A.

tonic firing while silencing proportionally many neurons increased the contributions of motif-classes capturing local dynamics (II, III, IX, X, XI) while decreasing those contributions capturing synchrony. The simplest result is that from Fig. 3D-F, as noise level increased, the ratios decreased, with the exception of motif-class I. We expected this exception, since motif-class I only measures the average spike rate across the raster, which was 0.5 even in the pure noise case. A series of test simulations with the associated characteristic neuronal activity patterns of motif-classes are depicted in Fig. C1.

5 Discussion

In this study, we apply the TCU theorem to spike rasters of neuronal networks. Through this, we show that the triple correlation is uniquely related to the network activity. We can deduce and group the motif-classes as shown in Fig. 1. We then examine how different types of motif-classes contribute to particular patterns (Table 1). Specifically, our simulation study reveals that certain motifs contribute more to the triple correlation than others (Table 1, Figs. 2 and 3). For instance, 'Divergence', 'Convergence', and 'Feedforward' motifs are strong potential contributors to the triple correlation, while 'Feedback', 'Synchrony', and 'Local Dynamics' are less important (Table 1). Overall, we establish the foundational nature of motifs in neural activity as up to three motifs characterize the entirety of the triple correlation. It is important to note that these motifs (defined in Table 1) are not examples taken from the literature, but instead directly arise from our analysis of the TCU theorem as applied to the spike raster!

While we show the importance of the third-order statistic, we want to emphasize that this metric includes lower-order statistics and that these lower-order metrics may also be important as well. For example, if both spatial lags are zero, the Fourier transform of the correlation (c_T) results in the bispectrum of a single location. This indicates that relationships between spectral components across frequency bands contribute to the description of the unique pattern

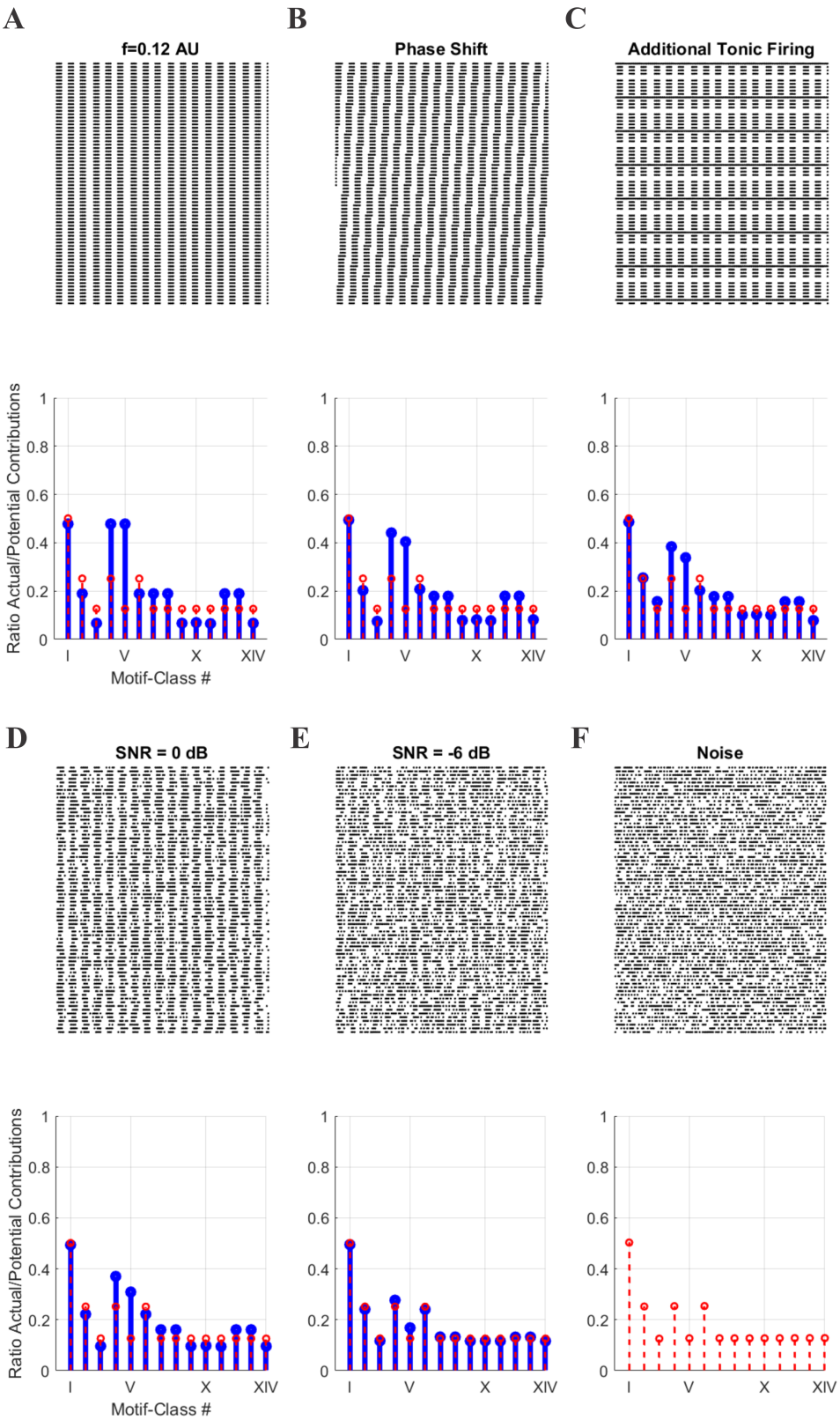

Figure 3: **Spike rasters and the relative contribution of motif-classes to the triple correlation.** The top two rows shows the analysis of periodic activity. In each panel, the raster plot of multi-unit spiking activity and the relative contribution (ratio of actual/potential contributions as shown in Fig. 2D) for each of the 14 motif-classes are shown. In the ratio plots, the blue lines show the ratio values for the corresponding raster plot above. The red dotted lines show the ratio values of only noise (replicated in Panel F). A) Frequency $f = 0.12$ AU. B) Same as Panel A with phase shift. C) Same as Panel A with additional tonic firing. The bottom two rows show the effect of noise. D) Same as in panel A with added noise SNR $= 0$dB. E) Same as in panel A with added noise SNR $= -6$dB. F) Noise only

in the neuronal activity. Frequency bands in different neurons also contribute: i.e. when one or both of the spatial lags are non-zero. Although the lower-order statistics may also be important, they do not fully characterize neuronal network activity, unlike the third-order statistic. Per the Wiener-Khinchin-Einstein Theorem, the Fourier transform of a channel's autocorrelation (second-order statistic) is the power spectrum (cf. van Drongelen, 2018). The power spectrum shows the impact of the activity of the frequency components, but the power spectrum does not provide information on the phase of these spectral components. In contrast, the triple correlation does include such phase information; indeed, this phase information in network activities (i.e. timing of activities) is critically important.

While the direct evaluation of the third-order correlation ($c_T(\nu_1, \tau_1, \nu_2, \tau_2)$) is not trivial, the conclusions we can further draw from the TCU theorem leads to powerful insights into the neuronal relationships that contribute to unique network activity patterns. Nonetheless, there are arbitrary aspects and limitations with this approach. For example, in keeping with raster plot convention, we converted the three-dimensional neuron positions into a one-dimensional array. The implicit assumption here is that the lags included in our correlation analysis cover the connectivity within the network. To generalize and avoid this constraint, we could also maintain the three-dimensional position, leading to a four-dimensional 'picture' (three for space and one for time), which would explicitly include neuronal interdistance. However, this addition would not change the essence of our claims that the TCU theorem governs uniqueness of patterns. While our proof only accounts for two-dimensional images, extending to higher dimensions would be a natural next step, just as our proof was itself a natural extension of Yellott & Iverson's (1992) proof.

In any case, once the neuron order in the raster is determined, it should remain fixed across comparisons of different patterns of that network. Given an arbitrary reduction from three dimensions to one, significant meaning should not be attached with the spatial lags (Equation (A1): ν_1, ν_2). In contrast, the temporal delays (Equation (A1): τ_1, τ_2) and their related frequency components (Equation (A1): ω_1, ω_2) do have meaning about the relative timing of activities.

Network motifs are already an important topic in neuronal network research (e.g. Sporns & Kötter, 2004), and their structures dictate fundamental signal analysis and processing by the neuronal networks. For example, Dechery & Maclean (2018) used graph theory to examine the functional network of V1 neurons in response to selective modulation; they found that the local population is able to predict individual neuron activity. EEG records provide a larger scale example, where the nodes represent cm-sized networks producing the signal at the macroelectrode, and the edges symbolize inter-network connections. In contrast, from microelectrode array recordings of cellular activities presented in raster plots, the node is defined by a neuron (single-unit traces) or a small set of neurons (multi-unit traces), and the edges are defined by direct or indirect connections.

It is important to note here that our analysis differs from the approach that studies have previously used to determine motif-classes. While some directly utilize structural data to derive pairwise connections, others infer functional networks from spiking activity across channels using pairwise relations such as cross-correlation or Granger causality (e.g. Bojanek et al., 2020; Dechery & Maclean, 2018; Schneidman et al., 2006; Jiang et al., 2017). In contrast, our motif-classes are determined from the triple correlation of the spike raster itself using combinations of temporal and spatial lags (Equation (1)). In each motif, the nodes represent neurons, and lags represent edges. From our approach, the triple correlation characterizes the neuronal network activity from the spike raster, defines motif-classes, and informs the importance of those different motif-classes. We also show that the three-point motif determines the uniqueness of the network.

Our claim that triple correlation of these rasters uniquely characterizes neuronal network activity rests on the assumption that the spike raster encompasses all essential activities of the network. For simplicity, we focused on B/W spike rasters, which means we have only incorporated spiking activity. This is not an issue in the simulations presented here because, by construction, the spiking captures all network activity. However, the same methodology can be applied to representations of network activity with a finite number of colors (see "Multicolored Images" in Yellott, 1993). Therefore, the network LFP may be included if the LFP is discretized to a limited set of colors. In clinical and experimental datasets, recorded spiking units typically significantly subsample the network; as such, LFP may be necessary to augment the spiking activity.

The clinical applications of the proposed approach abound. For example, network analysis of EEG (the macroscopic record of the field potential) activity is critical to support surgical planning in patients with epilepsy (e.g., Goodfellow er al., 2016; Hebbink et al, 2017). By discretizing the EEG signal, we can apply our analysis. For these reasons, we plan to apply this methodology to multi-unit spiking data from microelectrode array recordings in order to further test and quantify the characterization power of network activity using the triple correlation.

Acknowledgements

S.S.D. is supported by University of Chicago MSTP Training Grant T32GM007281. G.S. is supported by the Pritzker Endowment for the Neurosciences.

References

H. Bartelt, A. W. Lohmann, and B. Wirnitzer. Phase and amplitude recovery from bispectra. *Applied Optics*, 23(18): 3121–3129, September 1984. doi:10.1364/AO.23.003121.

K. Bojanek, Y. Zhu, and J. MacLean. Cyclic transitions between higher order motifs underlie sustained asynchronous spiking in sparse recurrent networks. *PLOS Computational Biology*, 16(9):e1007409, September 2020. doi:10.1371/journal.pcbi.1007409.

S. V. Canavan, T. L. Eissa, C. Schevon, G. M. McKhan, R. R. Goodman, R. G. Emerson, and W. van Drongelen. Epileptogenic Networks: Applying Network Analysis Techniques to Human Seizure Activity. In B. S. Bhattacharya and F. N. Chowdhury, editors, *Validating Neuro-Computational Models of Neurological and Psychiatric Disorders*, Springer Series in Computational Neuroscience, pages 293–312. Springer International Publishing, Cham, 2015. doi:10.1007/978-3-319-20037-8_11.

J. B. Dechery and J. N. MacLean. Functional triplet motifs underlie accurate predictions of single-trial responses in populations of tuned and untuned V1 neurons. *PLOS Computational Biology*, 14(5):e1006153, May 2018. doi:10.1371/journal.pcbi.1006153.

S. Foxley, V. Sampathkumar, V. De Andrade, S. Trinkle, A. Sorokina, K. Norwood, P. La Riviere, and N. Kasthuri. Multi-modal imaging of a single mouse brain over five orders of magnitude of resolution. *NeuroImage*, 238:118250, September 2021. doi:10.1016/j.neuroimage.2021.118250.

M. Goodfellow, C. Rummel, E. Abela, M. P. Richardson, K. Schindler, and J. R. Terry. Estimation of brain network ictogenicity predicts outcome from epilepsy surgery. *Scientific Reports*, 6:29215, July 2016. doi:10.1038/srep29215.

B. He and Z. Liu. Multimodal functional neuroimaging: integrating functional MRI and EEG/MEG. *IEEE reviews in biomedical engineering*, 1:23–40, 2008. doi:10.1109/RBME.2008.2008233.

J. Hebbink, H. Meijer, G. Huiskamp, S. van Gils, and F. Leijten. Phenomenological network models: Lessons for epilepsy surgery. *Epilepsia*, 58(10):e147–e151, October 2017. doi:10.1111/epi.13861.

M. Jiang, X. Gao, H. An, H. Li, and B. Sun. Reconstructing complex network for characterizing the time-varying causality evolution behavior of multivariate time series. *Scientific Reports*, 7(1):10486, September 2017. doi:10.1038/s41598-017-10759-3.

S. Jovanovi and S. Rotter. Interplay between Graph Topology and Correlations of Third Order in Spiking Neuronal Networks. *PLOS Computational Biology*, 12(6):e1004963, June 2016. doi:10.1371/journal.pcbi.1004963.

B. Julesz, E. N. Gilbert, L. A. Shepp, and H. L. Frisch. Inability of humans to discriminate between visual textures that agree in second-order statistics-revisited. *Perception*, 2(4):391–405, 1973. doi:10.1068/p020391.

B. Julesz. Visual Pattern Discrimination. *IRE Transactions on Information Theory*, 8(2):84–92, February 1962. doi:10.1109/TIT.1962.1057698.

R. Milo, S. Shen-Orr, S. Itzkovitz, N. Kashtan, D. Chklovskii, and U. Alon. Network Motifs: Simple Building Blocks of Complex Networks. *Science*, 298(5594):824–827, October 2002. doi:10.1126/science.298.5594.824.

Z. Moszner. Sur l'équation f(x)f(y)f(xy)=g(x)g(y)g(xy). *aequationes mathematicae*, 21(1):20–32, December 1980. doi:10.1007/BF02189336.

C. Rossant, S. Leijon, A. K. Magnusson, and R. Brette. Sensitivity of Noisy Neurons to Coincident Inputs. *Journal of Neuroscience*, 31(47):17193–17206, November 2011. doi:10.1523/JNEUROSCI.2482-11.2011.

E. Schneidman, M. J. Berry, R. Segev, and W. Bialek. Weak pairwise correlations imply strongly correlated network states in a neural population. *Nature*, 440(7087):1007–1012, April 2006. doi:10.1038/nature04701.

O. Sporns and R. Kötter. Motifs in Brain Networks. *PLoS Biology*, 2(11):e369, October 2004. doi:10.1371/journal.pbio.0020369.

T. Tchumatchenko, T. Geisel, M. Volgushev, and F. Wolf. Spike Correlations What Can They Tell About Synchrony? *Frontiers in Neuroscience*, 0, 2011. doi:10.3389/fnins.2011.00068.

W. van Drongelen. *Signal processing for neuroscientists: Introduction to the analysis of physiological signals.* Elsevier/Academic Press, 2nd edition edition, 2018.

J. I. Yellott. Implications of triple correlation uniqueness for texture statistics and the Julesz conjecture. *Journal of the Optical Society of America A*, 10(5):777–793, May 1993. doi:10.1364/JOSAA.10.000777.

J. I. Yellott and G. J. Iverson. Uniqueness properties of higher-order autocorrelation functions. *Journal of the Optical Society of America A*, 9(3):388–404, March 1992. doi:10.1364/JOSAA.9.000388.

S. Yu, H. Yang, H. Nakahara, G. S. Santos, D. Nikoli, and D. Plenz. Higher-Order Interactions Characterized in Cortical Activity. *Journal of Neuroscience*, 31(48):17514–17526, November 2011. doi:10.1523/JNEUROSCI.3127-11.2011.

Z. D. Zhang and M. J. Chacron. Adaptation to second order stimulus features by electrosensory neurons causes ambiguity. *Scientific Reports*, 6(1):28716, June 2016. doi:10.1038/srep28716.

Supporting Materials

A Uniqueness of Triple-Correlation for Network Spiking Activity

We represent neuronal activity as a typical two-dimensional raster, $x(n,t)$, where n is neuron location and t is time. We assume that the raster is a binary (black and white, cf. Figure 1), meaning $x(n,t)=1$ if neuron n fires at time t, and $x(n,t)=0$ otherwise. We note that everything below works just as well for any finite number of color (Yellot and Iverson, 1992), such as would be the case with discretized local field potential or EEG recordings. Even a colorful raster is still an image.

The triple correlation of $x(n,t)$ is

$$c_T(\nu_1,\tau_1,\nu_2,\tau_2)=\iint x(n,t)\,x(n+\nu_1,t+\tau_1)\,x(n+\nu_2,t+\tau_2)\,dn\,dt \tag{A1}$$

for spatial lags ν_1,ν_2 and temporal lags τ_1,τ_2. This is the triple correlation function that the TCU theorem shows uniquely characterizes the spike raster.

We define $\mathscr{F}[c_T]=C_T\leftrightarrow c_T$ as the Fourier transform of c_T

$$C_T(\sigma_1,\omega_1,\sigma_2,\omega_2)=\iiiint c_T(\nu_1,\tau_1,\nu_2,\tau_2)e^{-j\sigma_1\nu_1}e^{-j\omega_1\tau_1}e^{-j\sigma_2\nu_2}e^{-j\omega_2\tau_2}\,d\nu_1\,d\tau_1\,d\nu_2\,d\tau_2 \tag{A2}$$

We can rewrite this integral in terms of the Fourier transform of x by substituting (A1) into (A2) and rearranging the integration order to find

$$C_T(\sigma_1,\omega_1,\sigma_2,\omega_2)= \iiiint x(n,t)\,x(n+\nu_2,t+\tau_2)\left[\iint x(n+\nu_1,t+\tau_1)e^{-j\sigma_1\nu_1}e^{-j\omega_1\tau_1}\,d\nu_1\,d\tau_1\right]e^{-j\sigma_2\nu_2}e^{-j\omega_2\tau_2}\,d\nu_2\,d\tau_2\,dn\,dt. \tag{A3}$$

The part in between the [...] in (A3) can be rewritten as $e^{j\omega_1 t}e^{j\sigma_1 n}X(\sigma_1,\omega_1)$, with $X(\sigma_1,\omega_1)$ denoting the two dimensional Fourier transform of $x(n,t)$. Similarly, the part of Equation (A3) for ν_2 and τ_2 and their double integral can be arranged to evaluate to $e^{j\omega_2 t}e^{j\sigma_2 n}X(\sigma_2,\omega_2)$. Substitution of these results in (A3) results in:

$$C_T(\sigma_1,\omega_1,\sigma_2,\omega_2)=X(\sigma_1,\omega_1)X(\sigma_2,\omega_2)\iint x(n,t)e^{j(\omega_1+\omega_2)t}e^{j(\sigma_1+\sigma_2)n}\,dn\,dt \tag{A4}$$

The double integral evaluates to $X(-\sigma_1-\sigma_2,-\omega_1-\omega_2)=X^*(\sigma_1+\sigma_2,\omega_1+\omega_2)$, where the asterisk denotes a complex conjugate. Thus we see that the Fourier transform of c_T is usual definition of the bispectrum

$$c_T(\nu_1,\tau_1,\nu_2,\tau_2)\leftrightarrow X(\sigma_1,\omega_1)X(\sigma_2,\omega_2)X^*(\sigma_1+\sigma_2,\omega_1+\omega_2), \tag{A5}$$

which is the third-order equivalent of the Wiener-Khinchin-Einstein theorem.

Since images have a finite support and all of the above integration limits are implicitly at $(-\infty,\infty)$, we can modify the results for finite support as outlined for the one-dimensional signals in the Supporting Materials. That is, we multiply the spatiotemporal domain data by a two-dimensional boxcar limited between $(-\Sigma,\Sigma,-\Omega,\Omega)$ (or any other window with that support): $x_b=xw$. The frequency domain results are then characterized by the Fourier transforms convolved (denoted by $\circledast$) with the boxcar's Fourier transform (W) (or that of the window applied) denoted by: $X_B=X\circledast W$. By using this notation, the results in equations (A1)–(A5) would be adapted by adding the b and B subscripts.

Yellott and Iverson (1992) show in a constructive proof that a finite image (in our case a spike raster of a finite size) can be uniquely reconstructed from its third-order correlation. These authors also show and discuss how this does not hold for images of infinite size. Here we do not further discuss this aspect because the size of a spike raster is always finite.

One critically important message of this paper is that the time domain's triple correlation and the corresponding bispectrum in the frequency domain uniquely determine the firing pattern of a network. Yellott (1993) presents this as the TCU theorem. If we apply Yellott's TCU theorem to a spike raster, we get the following.

Theorem 1. *If* $x(n,t)$ *is a raster with bounded support and another raster* $y(n,t)$ *has the same triple correlation function as that of* x*, then* $y(n,t)=x(n+a,t+b)$ *for a pair of constants* a,b.

Here we extend the reasoning in Yellott's (1993) proof in one-dimension to present a simplified proof for a two-dimensional spatiotemporal case. Also see Moszner (1980) for additional rigor in the one dimensional case.

B Proof of Theorem 1 in two dimensions

Proof. Given the equality of third-order correlation functions, we can use Equation (A5) to find that

$$X(\sigma_1,\omega_1)X(\sigma_2,\omega_2)X(-\sigma_1-\sigma_2,-\omega_1-\omega_2) = Y(\sigma_1,\omega_1)Y(\sigma_2,\omega_2)Y(-\sigma_1-\sigma_2,-\omega_1-\omega_2) \tag{B1}$$

To borrow some convenient results from probability theory, we note that X and Y can be considered characteristic functions since we can consider x and y probability distributions: as finite images, x and y are bounded and nonnegative, and without loss of generality we can normalize them such that their integral is 1. Characteristic functions (the Fourier transforms of probability distributions) have two properties that are convenient for our purposes, the first of which is that they are non-zero in a region around the origin, thus allowing us the following division (for a rigorous treatment in the one dimensional case, cf. Moszner, 1980):

$$\frac{X(\sigma_1,\omega_1)X(\sigma_2,\omega_2)}{Y(\sigma_1,\omega_1)Y(\sigma_2,\omega_2)} = \frac{Y(-\sigma_1-\sigma_2,-\omega_1-\omega_2)}{X(-\sigma_1-\sigma_2,-\omega_1-\omega_2)}. \tag{B2}$$

Next we rewrite both complex functions in terms of their amplitude and phase, i.e. $X(\sigma,\omega) = |X(\sigma,\omega)|e^{j\phi(X(\sigma,\omega))}$, where ϕ gives the phase. So then we can rewrite the right-hand side of (B2)

$$\frac{X(\sigma_1,\omega_1)X(\sigma_2,\omega_2)}{Y(\sigma_1,\omega_1)Y(\sigma_2,\omega_2)} = \frac{|Y(-\sigma_1-\sigma_2,-\omega_1-\omega_2)|e^{j\phi(Y(-\sigma_1-\sigma_2,-\omega_1-\omega_2))}}{|X(-\sigma_1-\sigma_2,-\omega_1-\omega_2)|e^{j\phi(X(-\sigma_1-\sigma_2,-\omega_1-\omega_2))}}. \tag{B3}$$

Here we use the second convenient property of characteristic functions, namely that they are Hermitian, i.e. $X(-\sigma,-\omega) = X^*(\sigma,\omega)$. By setting $\sigma_2 = 0, \omega_2 = 0$ in (B3), we can use this Hermitian property to derive the fact that $|X(\sigma_1,\omega_1)|^2 = |Y(\sigma_1,\omega_1)|^2$ for any σ_1,ω_1. In particular, $|X(-\sigma_1-\sigma_2,-\omega_1-\omega_2)| = |Y(-\sigma_1-\sigma_2,-\omega_1-\omega_2)|$ so we can flip those terms.

$$= \frac{|X(-\sigma_1-\sigma_2,-\omega_1-\omega_2)|e^{j\phi(Y(-\sigma_1-\sigma_2,-\omega_1-\omega_2))}}{|Y(-\sigma_1-\sigma_2,-\omega_1-\omega_2)|e^{j\phi(X(-\sigma_1-\sigma_2,-\omega_1-\omega_2))}} \tag{B4}$$

We can also rewrite those same terms thanks to the same Hermitian property.

$$= \frac{|X^*(\sigma_1+\sigma_2,\omega_1+\omega_2)|e^{j\phi(Y^*(-\sigma_1-\sigma_2,-\omega_1-\omega_2))}}{|Y^*(\sigma_1+\sigma_2,\omega_1+\omega_2)|e^{j\phi(X^*(-\sigma_1-\sigma_2,-\omega_1-\omega_2))}} \tag{B5}$$

Simple complex properties are $|X| = |X^*|$ and $\phi(X) = -\phi(X^*)$, which give us

$$= \frac{|X(\sigma_1+\sigma_2,\omega_1+\omega_2)|e^{j\phi(X(\sigma_1+\sigma_2,\omega_1+\omega_2))}}{|Y(\sigma_1+\sigma_2,\omega_1+\omega_2)|e^{j\phi(Y(\sigma_1+\sigma_2,\omega_1+\omega_2))}} \tag{B6}$$

Next, we return from the amplitude and phase notation to the complex functions themselves:

$$= \frac{X(\sigma_1+\sigma_2,\omega_1+\omega_2)}{Y(\sigma_1+\sigma_2,\omega_1+\omega_2)}. \tag{B7}$$

Now we define $H(\sigma,\omega) = \frac{X(\sigma,\omega)}{Y(\sigma,\omega)}$ so we can rewrite (B7) as

$$H(\sigma_1,\omega_1)H(\sigma_2,\omega_2) = H(\sigma_1+\sigma_2,\omega_1+\omega_2). \tag{B8}$$

Therefore by a basic result of complex analysis $H(\sigma,\omega) = e^{j(k\sigma+l\omega)}$, and thus

$$Y(\sigma,\omega) = X(\sigma,\omega)e^{j(k\sigma+l\omega)}. \tag{B9}$$

This holds in a region near the origin, and another property of characteristic functions is that, if their probability distribution has finite support, the probability distribution is uniquely determined by the value of the characteristic function in a region of the origin. Thus, in the spatiotemporal domain,

$$y(n,t) = x(n+k,t+l) \text{with constants } k,l. \tag{B10}$$

□

C Test simulations for the triple correlation algorithm

We tested the triple correlation algorithm by simulating rasters of each neuronal processing property as listed in Table 1. The representative motif-classes and their associated relative contributions to the triple correlations are shown in Fig. C1.

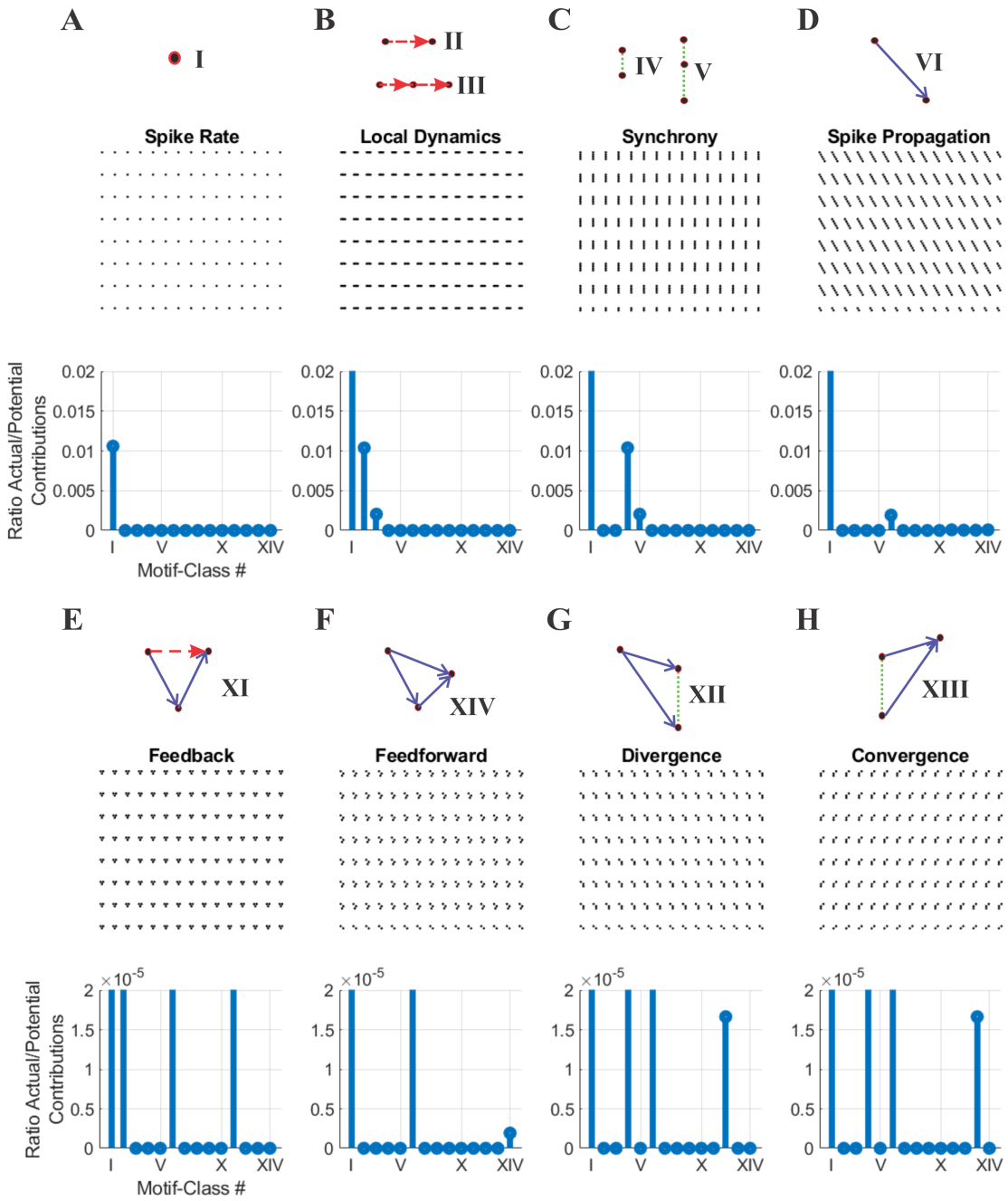

Figure C1: **Test spike rasters of neuronal processing properties and the relative contribution of motif-classes to the triple correlation.** In each panel, the top row shows the characteristic motif-classes and spike raster, and the bottom row shows the ratios between the actual and potential contributions for each of the 14 motif-classes. A) Motif-class I corresponds to Spike Rate. B) Motif-classes II/III correspond to Local Dynamics. C) Motif-classes IV/V correspond to Synchrony. D) Motif-class VI corresponds to Spike Propagation. E) Motif-class XI corresponds to Feedback. F) Motif-class XIV corresponds to Feedforward. G) Motif-class XII corresponds to Divergence. H) Motif-class XIII corresponds to Convergence.

Table D1: Given 3 possible time bins and 3 possible neurons, the number of possible orderings in space and time can be determined by the following table.

		# different neurons		
		3	2	1
# different time bins	3	A	B	C
	2	B	D	E
	1	C	E	F

D The number of qualitatively distinct spike motifs

Given three distinct nodes, we want to know how many ways there are to order them in time and space, with the caveat that we may also place one node on top of another in either time, or space, or both. To count this, we divide the cases according to how many different time bins and neurons the nodes have between them. For example, if all the nodes are completely distinct in time and space, then there are both three neurons and three time bins between the three nodes. On the other hand, if we overlap all three nodes in both time and space, then there is only one neuron and one time bin between them. All the cases are labelled in Table D1. Note that the cases are symmetric, so we will calculate the values as if in the lower left half of the matrix, i.e. where the number of neurons is greater than or equal to the number of time bins.

A. In the case where no nodes share a neuron, there are 3! ways to order them in space. Similarly if the nodes share no time bins, then there are 3! ways to order the time bins. So, if no neurons nor time bins are shared, then there are $3!3! = 36$ orderings.
B. Given that the nodes only have two distinct neurons between them, there are three ways to choose which nodes share the same neuron, and then two ways to choose whether the remaining node has a neuron before or after the identical nodes neuron, for $3 \cdot 2 = 6$ spatial orderings. As above, if no time bins are identical, then there are 3! temporal orderings. So there are $3 \cdot 2 \cdot 3! = 36$ orderings.
C. If nodes share the same neuron, then there is only one way to order that neuron. As above, if no time bins are identical then there are 3! temporal orderings, giving a total of $1 \cdot 3! = 6$ orderings.
D. We already established that for the case where two neurons are the same, there are $3 \cdot 2 = 6$ orderings. The same is true when the nodes only have two distinct time bins. So there are $3 \cdot 2 \cdot 3 \cdot 2 = 36$ orderings.
E. We already established that for the case where two neurons are the same, there are $3 \cdot 2 = 6$ orderings, and for the case where all time bins are the same, there is only one ordering. So there are $3 \cdot 2 \cdot 1 = 6$ orderings.
F. In the case where all neurons and all time bins are the same, there is only one ordering.

We sum up the table: $A + 2B + 2C + D + 2E + F = 36 + 2 \cdot 36 + 2 \cdot 6 + 36 + 2 \cdot 6 + 1 = 169$

Table D2: **Motif-classes for triple correlation with different spatial and temporal lags.** The 169 motif-classes for three-node motifs with different lags. Each row represents a single three-node motif class, where the base node implicitly has lags $n_0 = 0$ and $t_0 = 0$. The four lags of the other two nodes (n_1, n_2, t_1, t_2) are the ones in Equation (1). In the lag columns, '0' entries denote that the lag is zero while '+' entries denote a positive value, and '-' entries denote a negative value (respectively greater or less than the base node's lag). Note that in case where one modality (space or time) shares the same (non-zero) sign, whether those two lags are identical or not qualitatively changes our interpretation of the spiking pattern.

Lag Motif	n_1	n_2	t_1	t_2	Constraints	Information Flow Pattern	Configuration
1	0	0	0	0		I	
2.1	0	0	0	+		II	
2.2	0	0	0	-		II	
3.1	0	0	+	0		II	
3.2	0	0	-	0		II	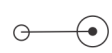

4.1.1	0	0	+	+	$\lvert t_1\rvert > \lvert t_2\rvert$	III	
4.1.2	0	0	+	+	$\lvert t_1\rvert < \lvert t_2\rvert$	III	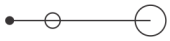
4.1.3	0	0	+	+	$\lvert t_1\rvert = \lvert t_2\rvert$	II	
4.2	0	0	+	-		III	
4.3	0	0	-	+		III	
4.4.1	0	0	-	-	$\lvert t_1\rvert > \lvert t_2\rvert$	III	
4.4.2	0	0	-	-	$\lvert t_1\rvert < \lvert t_2\rvert$	III	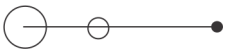
4.4.3	0	0	-	-	$\lvert t_1\rvert = \lvert t_2\rvert$	II	
5.1	0	+	0	0		IV	
5.2	0	-	0	0		IV	
6.1	0	+	0	+		VI	
6.2	0	+	0	-		VI	
6.3	0	-	0	+		VI	
6.4	0	-	0	-		VI	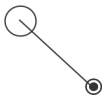
7.1	0	+	+	0		VII	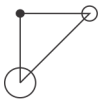
7.2	0	+	-	0		VIII	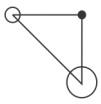
7.3	0	-	+	0		VII	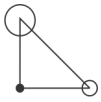
7.4	0	-	-	0		VIII	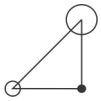

8.1.1	0	+	+	+	$\lvert t_1\rvert > \lvert t_2\rvert$	XI	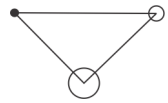
8.1.2	0	+	+	+	$\lvert t_1\rvert < \lvert t_2\rvert$	X	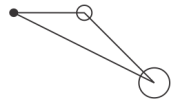
8.1.3	0	+	+	+	$\lvert t_1\rvert = \lvert t_2\rvert$	VIII	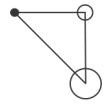
8.2	0	+	+	-		IX	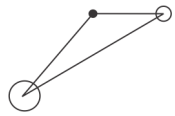
8.3	0	+	-	+		X	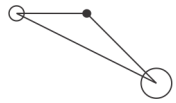
8.4.1	0	+	-	-	$\lvert t_1\rvert > \lvert t_2\rvert$	XI	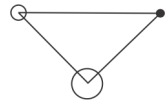
8.4.2	0	+	-	-	$\lvert t_1\rvert < \lvert t_2\rvert$	IX	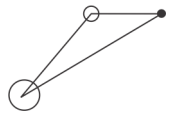
8.4.3	0	+	-	-	$\lvert t_1\rvert = \lvert t_2\rvert$	VII	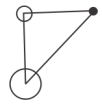
8.5.1	0	-	+	+	$\lvert t_1\rvert > \lvert t_2\rvert$	XI	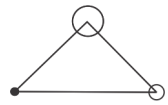
8.5.2	0	-	+	+	$\lvert t_1\rvert < \lvert t_2\rvert$	X	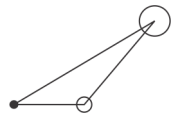
8.5.3	0	-	+	+	$\lvert t_1\rvert = \lvert t_2\rvert$	VIII	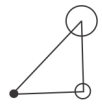
8.6	0	-	+	-		IX	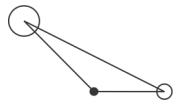
8.7	0	-	-	+		X	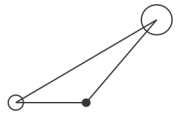
8.8.1	0	-	-	-	$\lvert t_1\rvert > \lvert t_2\rvert$	XI	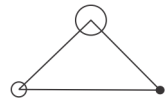

8.8.2	0	-	-	-	$\lvert t_1 \rvert < \lvert t_2 \rvert$	IX	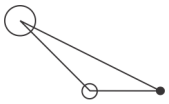
8.8.3	0	-	-	-	$\lvert t_1 \rvert = \lvert t_2 \rvert$	VII	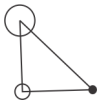
9.1	+	0	0	0		IV	
9.2	-	0	0	0		IV	
10.1	+	0	0	+		VII	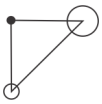
10.2	+	0	0	-		VIII	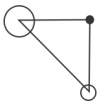
10.3	-	0	0	+		VII	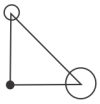
10.4	-	0	0	-		VIII	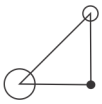
11.1	+	0	+	0		VI	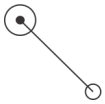
11.2	+	0	-	0		VI	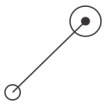
11.3	-	0	+	0		VI	
11.4	-	0	-	0		VI	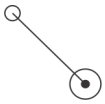
12.1.1	+	0	+	+	$\lvert t_1 \rvert > \lvert t_2 \rvert$	X	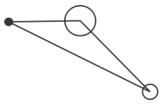
12.1.2	+	0	+	+	$\lvert t_1 \rvert < \lvert t_2 \rvert$	XI	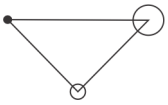

12.1.3	+	0	+	+	$\lvert t_1\rvert = \lvert t_2\rvert$	VIII	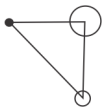
12.2	+	0	+	-		X	
12.3	+	0	-	+		IX	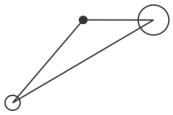
12.4.1	+	0	-	-	$\lvert t_1\rvert > \lvert t_2\rvert$	IX	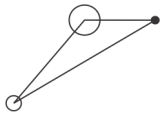
12.4.2	+	0	-	-	$\lvert t_1\rvert < \lvert t_2\rvert$	XI	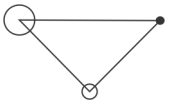
12.4.3	+	0	-	-	$\lvert t_1\rvert = \lvert t_2\rvert$	VII	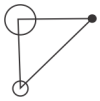
12.5.1	-	0	+	+	$\lvert t_1\rvert > \lvert t_2\rvert$	X	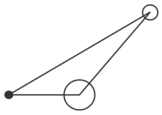
12.5.2	-	0	+	+	$\lvert t_1\rvert < \lvert t_2\rvert$	XI	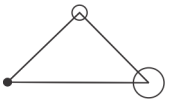
12.5.3	-	0	+	+	$\lvert t_1\rvert = \lvert t_2\rvert$	VIII	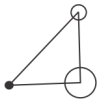
12.6	-	0	+	-		X	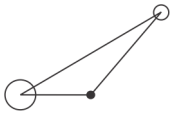
12.7	-	0	-	+		IX	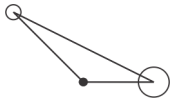
12.8.1	-	0	-	-	$\lvert t_1\rvert > \lvert t_2\rvert$	IX	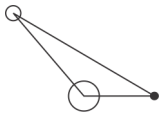
12.8.2	-	0	-	-	$\lvert t_1\rvert < \lvert t_2\rvert$	XI	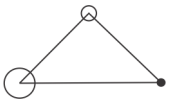

12.8.3	-	0	-	-	$\lvert t_1\rvert = \lvert t_2\rvert$	VII	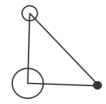
13.1.1	+	+	0	0	$\lvert n_1\rvert > \lvert n_2\rvert$	V	
13.1.2	+	+	0	0	$\lvert n_1\rvert < \lvert n_2\rvert$	V	
13.1.3	+	+	0	0	$\lvert n_1\rvert = \lvert n_2\rvert$	IV	
13.2	+	-	0	0		V	
13.3	-	+	0	0		V	
13.4.1	-	-	0	0	$\lvert n_1\rvert > \lvert n_2\rvert$	V	
13.4.2	-	-	0	0	$\lvert n_1\rvert < \lvert n_2\rvert$	V	
13.4.3	-	-	0	0	$\lvert n_1\rvert = \lvert n_2\rvert$	IV	
14.1.1	+	+	0	+	$\lvert n_1\rvert > \lvert n_2\rvert$	XIII	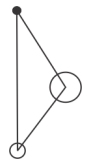

14.1.2	+	+	0	+	$\lvert n_1 \rvert < \lvert n_2 \rvert$	XIII	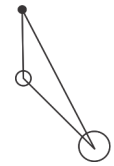
14.1.3	+	+	0	+	$\lvert n_1 \rvert = \lvert n_2 \rvert$	VII	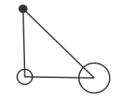
14.2.1	+	+	0	-	$\lvert n_1 \rvert > \lvert n_2 \rvert$	XII	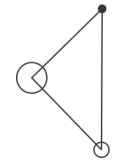
14.2.2	+	+	0	-	$\lvert n_1 \rvert < \lvert n_2 \rvert$	XII	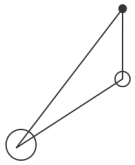
14.2.3	+	+	0	-	$\lvert n_1 \rvert = \lvert n_2 \rvert$	VIII	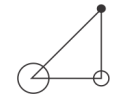
14.3	+	-	0	+		XIII	
14.4	+	-	0	-		XII	
14.5	-	+	0	+		XIII	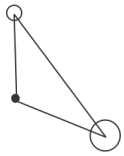
14.6	-	+	0	-		XII	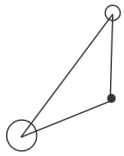
14.7.1	-	-	0	+	$\lvert n_1 \rvert > \lvert n_2 \rvert$	XIII	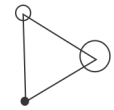

14.7.2	-	-	0	+	$\lvert n_1 \rvert < \lvert n_2 \rvert$	XIII	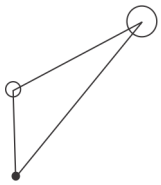
14.7.3	-	-	0	+	$\lvert n_1 \rvert = \lvert n_2 \rvert$	VII	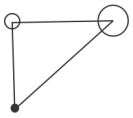
14.8.1	-	-	0	-	$\lvert n_1 \rvert > \lvert n_2 \rvert$	XII	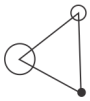
14.8.2	-	-	0	-	$\lvert n_1 \rvert < \lvert n_2 \rvert$	XII	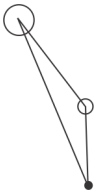
14.8.3	-	-	0	-	$\lvert n_1 \rvert = \lvert n_2 \rvert$	VIII	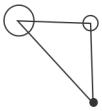
15.1.1	+	+	+	0	$\lvert n_1 \rvert > \lvert n_2 \rvert$	XIII	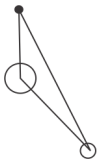
15.1.2	+	+	+	0	$\lvert n_1 \rvert < \lvert n_2 \rvert$	XIII	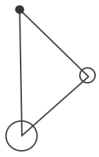
15.1.3	+	+	+	0	$\lvert n_1 \rvert = \lvert n_2 \rvert$	VII	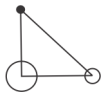
15.2.1	+	+	-	0	$\lvert n_1 \rvert > \lvert n_2 \rvert$	XII	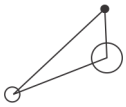
15.2.2	+	+	-	0	$\lvert n_1 \rvert < \lvert n_2 \rvert$	XII	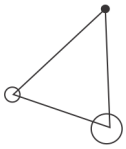
15.2.3	+	+	-	0	$\lvert n_1 \rvert = \lvert n_2 \rvert$	VIII	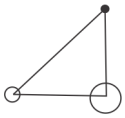

15.3	+	-	+	0		XIII	
15.4	+	-	-	0		XII	
15.5	-	+	+	0		XIII	
15.6	-	+	-	0		XII	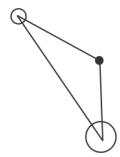
15.7.1	-	-	+	0	$\lvert n_1 \rvert > \lvert n_2 \rvert$	XIII	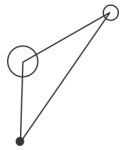
15.7.2	-	-	+	0	$\lvert n_1 \rvert < \lvert n_2 \rvert$	XIII	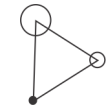
15.7.3	-	-	+	0	$\lvert n_1 \rvert = \lvert n_2 \rvert$	VII	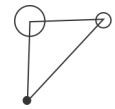
15.8.1	-	-	-	0	$\lvert n_1 \rvert > \lvert n_2 \rvert$	XII	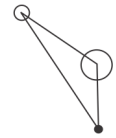
15.8.2	-	-	-	0	$\lvert n_1 \rvert < \lvert n_2 \rvert$	XII	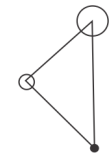
15.8.3	-	-	-	0	$\lvert n_1 \rvert = \lvert n_2 \rvert$	VIII	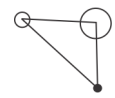

16.1.1	+	+	+	+	$\lvert n_1\rvert > \lvert n_2\rvert$ $\lvert t_1\rvert > \lvert t_2\rvert$	XIV	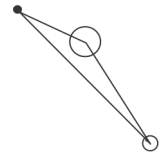
16.1.2	+	+	+	+	$\lvert n_1\rvert > \lvert n_2\rvert$ $\lvert t_1\rvert < \lvert t_2\rvert$	XIV	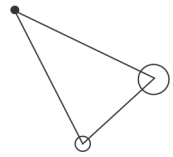
16.1.3	+	+	+	+	$\lvert n_1\rvert > \lvert n_2\rvert$ $\lvert t_1\rvert = \lvert t_2\rvert$	XII	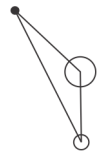
16.1.4	+	+	+	+	$\lvert n_1\rvert < \lvert n_2\rvert$ $\lvert t_1\rvert > \lvert t_2\rvert$	XIV	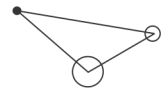
16.1.5	+	+	+	+	$\lvert n_1\rvert < \lvert n_2\rvert$ $\lvert t_1\rvert < \lvert t_2\rvert$	XIV	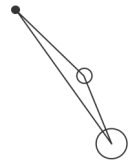
16.1.6	+	+	+	+	$\lvert n_1\rvert < \lvert n_2\rvert$ $\lvert t_1\rvert = \lvert t_2\rvert$	XII	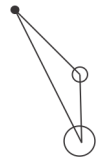
16.1.7	+	+	+	+	$\lvert n_1\rvert = \lvert n_2\rvert$ $\lvert t_1\rvert > \lvert t_2\rvert$	IX	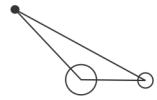
16.1.8	+	+	+	+	$\lvert n_1\rvert = \lvert n_2\rvert$ $\lvert t_1\rvert < \lvert t_2\rvert$	IX	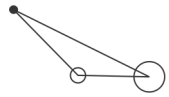
16.1.9	+	+	+	+	$\lvert n_1\rvert = \lvert n_2\rvert$ $\lvert t_1\rvert = \lvert t_2\rvert$	VI	
16.2.1	+	+	+	-	$\lvert n_1\rvert > \lvert n_2\rvert$	XIV	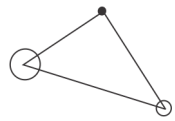
16.2.2	+	+	+	-	$\lvert n_1\rvert < \lvert n_2\rvert$	XIV	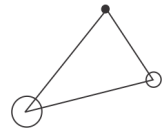
16.2.3	+	+	+	-	$\lvert n_1\rvert = \lvert n_2\rvert$	XI	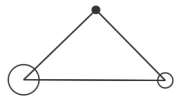

16.3.1	+	+	-	+	$\lvert n_1\rvert > \lvert n_2\rvert$	XIV	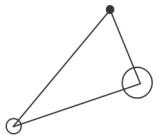
16.3.2	+	+	-	+	$\lvert n_1\rvert < \lvert n_2\rvert$	XIV	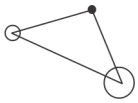
16.3.3	+	+	-	+	$\lvert n_1\rvert = \lvert n_2\rvert$	XI	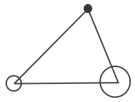
16.4.1	+	+	-	-	$\lvert n_1\rvert > \lvert n_2\rvert$ $\lvert t_1\rvert > \lvert t_2\rvert$	XIV	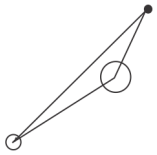
16.4.2	+	+	-	-	$\lvert n_1\rvert > \lvert n_2\rvert$ $\lvert t_1\rvert < \lvert t_2\rvert$	XIV	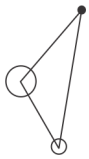
16.4.3	+	+	-	-	$\lvert n_1\rvert > \lvert n_2\rvert$ $\lvert t_1\rvert = \lvert t_2\rvert$	XIII	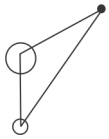
16.4.4	+	+	-	-	$\lvert n_1\rvert < \lvert n_2\rvert$ $\lvert t_1\rvert > \lvert t_2\rvert$	XIV	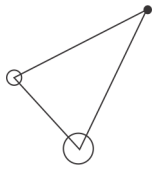
16.4.5	+	+	-	-	$\lvert n_1\rvert < \lvert n_2\rvert$ $\lvert t_1\rvert < \lvert t_2\rvert$	XIV	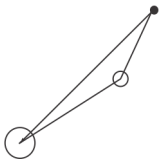
16.4.6	+	+	-	-	$\lvert n_1\rvert < \lvert n_2\rvert$ $\lvert t_1\rvert = \lvert t_2\rvert$	XIII	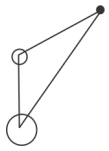
16.4.7	+	+	-	-	$\lvert n_1\rvert = \lvert n_2\rvert$ $\lvert t_1\rvert > \lvert t_2\rvert$	X	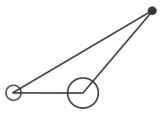
16.4.8	+	+	-	-	$\lvert n_1\rvert = \lvert n_2\rvert$ $\lvert t_1\rvert < \lvert t_2\rvert$	X	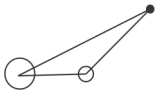

16.4.9	+	+	-	-	$\lvert n_1\rvert = \lvert n_2\rvert$ $\lvert t_1\rvert = \lvert t_2\rvert$	VI	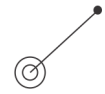
16.5.1	+	-	+	+	$\lvert t_1\rvert > \lvert t_2\rvert$	XIV	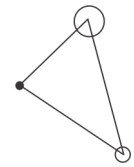
16.5.2	+	-	+	+	$\lvert t_1\rvert < \lvert t_2\rvert$	XIV	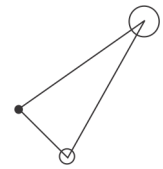
16.5.3	+	-	+	+	$\lvert t_1\rvert = \lvert t_2\rvert$	XII	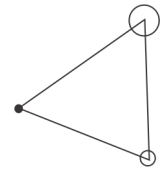
16.6	+	-	+	-		XIV	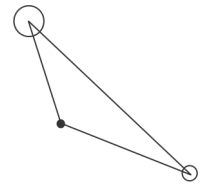
16.7	+	-	-	+		XIV	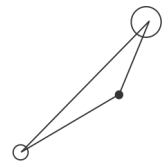
16.8.1	+	-	-	-	$\lvert t_1\rvert > \lvert t_2\rvert$	XIV	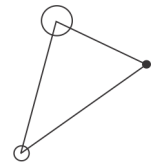
16.8.2	+	-	-	-	$\lvert t_1\rvert < \lvert t_2\rvert$	XIV	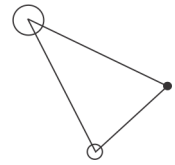
16.8.3	+	-	-	-	$\lvert t_1\rvert = \lvert t_2\rvert$	XIII	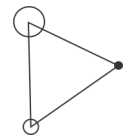
16.9.1	-	+	+	+	$\lvert t_1\rvert > \lvert t_2\rvert$	XIV	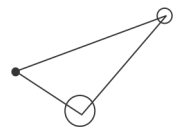

16.9.2	-	+	+	+	$\lvert t_1\rvert < \lvert t_2\rvert$	XIV	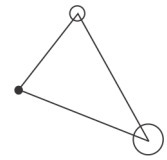
16.9.3	-	+	+	+	$\lvert t_1\rvert = \lvert t_2\rvert$	XII	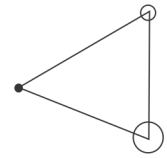
16.10	-	+	+	-		XIV	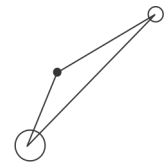
16.11	-	+	-	+		XIV	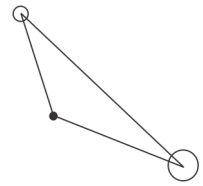
16.12.1	-	+	-	-	$\lvert t_1\rvert > \lvert t_2\rvert$	XIV	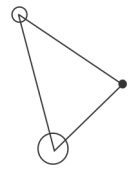
16.12.2	-	+	-	-	$\lvert t_1\rvert < \lvert t_2\rvert$	XIV	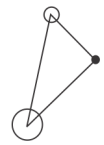
16.12.3	-	+	-	-	$\lvert t_1\rvert = \lvert t_2\rvert$	XIII	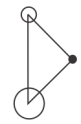
16.13.1	-	-	+	+	$\lvert n_1\rvert > \lvert n_2\rvert$ $\lvert t_1\rvert > \lvert t_2\rvert$	XIV	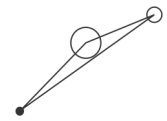
16.13.2	-	-	+	+	$\lvert n_1\rvert > \lvert n_2\rvert$ $\lvert t_1\rvert < \lvert t_2\rvert$	XIV	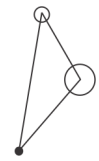
16.13.3	-	-	+	+	$\lvert n_1\rvert > \lvert n_2\rvert$ $\lvert t_1\rvert = \lvert t_2\rvert$	XII	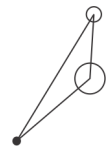

16.13.4	-	-	+	+	$\lvert n_1\rvert < \lvert n_2\rvert$ $\lvert t_1\rvert > \lvert t_2\rvert$	XIV	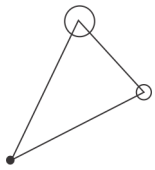
16.13.5	-	-	+	+	$\lvert n_1\rvert < \lvert n_2\rvert$ $\lvert t_1\rvert < \lvert t_2\rvert$	XIV	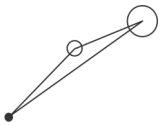
16.13.6	-	-	+	+	$\lvert n_1\rvert < \lvert n_2\rvert$ $\lvert t_1\rvert = \lvert t_2\rvert$	XII	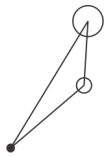
16.13.7	-	-	+	+	$\lvert n_1\rvert = \lvert n_2\rvert$ $\lvert t_1\rvert > \lvert t_2\rvert$	IX	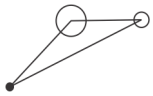
16.13.8	-	-	+	+	$\lvert n_1\rvert = \lvert n_2\rvert$ $\lvert t_1\rvert < \lvert t_2\rvert$	IX	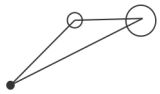
16.13.9	-	-	+	+	$\lvert n_1\rvert = \lvert n_2\rvert$ $\lvert t_1\rvert = \lvert t_2\rvert$	VI	
16.14.1	-	-	+	-	$\lvert n_1\rvert > \lvert n_2\rvert$	XIV	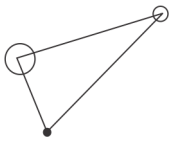
16.14.2	-	-	+	-	$\lvert n_1\rvert < \lvert n_2\rvert$	XIV	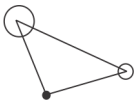
16.14.3	-	-	+	-	$\lvert n_1\rvert = \lvert n_2\rvert$	XI	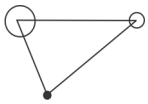
16.15.1	-	-	-	+	$\lvert n_1\rvert > \lvert n_2\rvert$	XIV	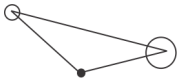
16.15.2	-	-	-	+	$\lvert n_1\rvert < \lvert n_2\rvert$	XIV	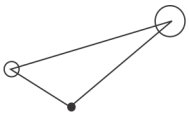
16.15.3	-	-	-	+	$\lvert n_1\rvert = \lvert n_2\rvert$	XI	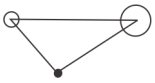
16.16.1	-	-	-	-	$\lvert n_1\rvert > \lvert n_2\rvert$ $\lvert t_1\rvert > \lvert t_2\rvert$	XIV	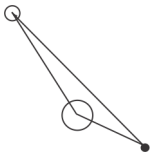

16.16.2	-	-	-	-	$\lvert n_1\rvert > \lvert n_2\rvert$ $\lvert t_1\rvert < \lvert t_2\rvert$	XIV	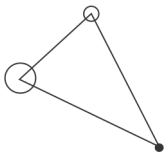
16.16.3	-	-	-	-	$\lvert n_1\rvert > \lvert n_2\rvert$ $\lvert t_1\rvert = \lvert t_2\rvert$	XIII	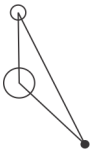
16.16.4	-	-	-	-	$\lvert n_1\rvert < \lvert n_2\rvert$ $\lvert t_1\rvert > \lvert t_2\rvert$	XIV	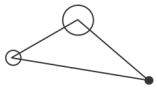
16.16.5	-	-	-	-	$\lvert n_1\rvert < \lvert n_2\rvert$ $\lvert t_1\rvert < \lvert t_2\rvert$	XIV	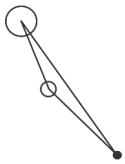
16.16.6	-	-	-	-	$\lvert n_1\rvert < \lvert n_2\rvert$ $\lvert t_1\rvert = \lvert t_2\rvert$	XIII	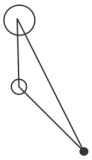
16.16.7	-	-	-	-	$\lvert n_1\rvert = \lvert n_2\rvert$ $\lvert t_1\rvert > \lvert t_2\rvert$	X	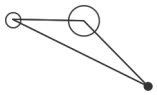
16.16.8	-	-	-	-	$\lvert n_1\rvert = \lvert n_2\rvert$ $\lvert t_1\rvert < \lvert t_2\rvert$	X	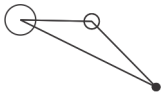
16.16.9	-	-	-	-	$\lvert n_1\rvert = \lvert n_2\rvert$ $\lvert t_1\rvert = \lvert t_2\rvert$	VI	